

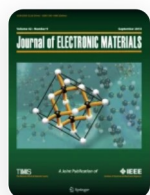
[Home](#) [Journal of Electronic Materials](#) [Article](#)


# Multivariate Analysis of a Cobalt Octaethyl Porphyrin-Functionalized SWNT Microsensor Device for Selective and Simultaneous Detection of Multiple Analytes

Original Research Article Published: 22 July 2021

Volume 50, pages 5780–5787, (2021) [Cite this article](#)[Download PDF](#) ↓

Access provided by Dr. Babasaheb Ambedkar Marathwada University, Aurangabad

[Journal of Electronic Materials](#)[Aims and scope](#)[Submit manuscript](#)

[Sumedh M. Shirsat](#), [Gajanan A. Bodkhe](#), [Minakshi M. Sonawane](#), [Bharti W. Gawali](#) & [Mahendra D. Shirsat](#) 

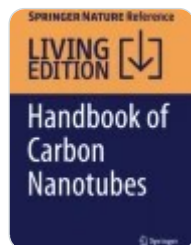
 364 Accesses  11 Citations [Explore all metrics](#) →

## Abstract

Multivariate analysis is carried out for single-walled carbon nanotubes (SWNTs) functionalized with a cobalt octaethyl porphyrin (CoOEP) chemiresistive sensor device for

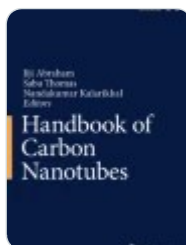
selective and simultaneous detection of multiple analytes. The chemiresistor was prepared on Si/SiO<sub>2</sub> substrate with photolithographically patterned gold microelectrodes having a 3- $\mu$ m gap. SWNTs were aligned dielectrophoretically and functionalized with CoOEP by drop-casting. The aligned and CoOEP-functionalized SWNTs were characterized with electrical (*I*-*V* method), structural, spectroscopic, and morphological techniques, and sensor performance was investigated in a chemiresistive sensing modality. The fabricated sensor shows response towards acetone, dichloromethane, methyl ethyl ketone, ethanol, and methanol, with a lower detection limit of 5 ppm, which is far below the OSHA permissible exposure limit for each analyte, and demonstrates fast response and recovery. The multivariate analysis viz. principal component analysis and linear discrimination analysis reveals high discriminating capability of SWNTs functionalized with the CoOEP chemiresistive sensor towards these analytes, which could be used as an intelligent electronic nose (E-nose). This type of intelligent E-nose can address the crucial need for monitoring environmental pollution in industries, homes, buildings, etc.

## Similar content being viewed by others



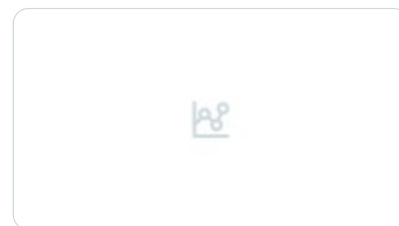
### Carbon Nanotubes for Sensing Applications

Chapter | © 2021



### Carbon Nanotubes for Sensing Applications

Chapter | © 2022



### POMs as Active Center for Sensitive Electrochemical Detection of Bisphenol ...

Article | 09 July 2019

[Use our pre-submission checklist](#) →

Avoid common mistakes on your manuscript.



# Introduction

---

Industrialization, urbanization, and deforestation have significantly increased environmental pollution levels, causing deterioration of soil, air, and water resources. Among all, air pollutants and volatile organic compounds (VOCs) have immensely threatened the environment and health of the living world due to their facile spreading. When looking back on history, many accidents have happened because of gas leaks: the Bhopal gas tragedy (1984) and the Vishakapatnam gas leak (May 2020) in India, the Beijing gas leak (December 2008) in China, and the gas leak in a Chinese mine (Nov 2011). To prevent these types of accidents and preserve the environment, gas detectors with an intelligent system, i.e. electronic nose (E-nose), with multivariate analysis can play a crucial role. An E-nose is a device that can sense odors or flavors much like mammals can. Intelligent E-noses are able to detect and differentiate based on the type of odor and can show the concentration of target gases using chemical gas sensor arrays.

Fabrication of E-noses is possible with good sensing materials. To date, various materials have been explored for gas sensors in different sensing modalities, including conducting polymers,<sup>1,2</sup> metal nanoparticles,<sup>3</sup> metal oxides,<sup>4</sup> carbon nanotubes,<sup>5</sup> graphene,<sup>6</sup> and porphyrins.<sup>7</sup> Each of these materials has certain issues such as selectivity, sensitivity, response and recovery time, facile operation, and cost-effective device fabrication. Single-walled carbon nanotubes (SWNTs) are a rolled single layer of a graphene sheet, which can be conducting or semiconducting based on its chirality and diameter.<sup>8</sup> SWNTs possess high a surface-to-volume ratio, hollow geometry, and ballistic charge conduction, and the effect of gas adsorption on conductivity makes them effective for microelectronic devices<sup>9</sup> for chemical gas sensing applications with high sensitivity and stability, but selectivity and lower recovery are crucial issues.<sup>10,11,12</sup> To tackle these issues, composite and functionalized SWNTs with active species like conducting polymers,<sup>13</sup> metal nanoparticles,<sup>14</sup> metal oxides,<sup>15</sup> nafion,<sup>16</sup> and porphyrins<sup>17,18</sup> have been explored, but these issues remain largely unresolved.

On the other hand, porphyrins are an interesting family of compounds due to their optical and structural properties and chemical stability.<sup>19</sup> The basic structure of porphyrins is formed by four pyrrolic rings linked with methynic bonds.<sup>20</sup> When in the free base, the porphyrin ring's

two hydrogen atoms replace with transition metal atoms, and are known as metalloporphyrins. Porphyrins have a wide range of interaction mechanisms for analyte binding, such as  $\pi$  bonds, weak Van der Waals forces for hydrogen bonding, and coordination with a central metal ion; these make porphyrins sensitive and selective for sensor applications.<sup>21</sup> Various porphyrins (free base and metal-centered) have been explored for gas-sensing applications in optical,<sup>22,23</sup> mass detection,<sup>24</sup> chemiresistive,<sup>25</sup> and chemical-sensitive field-effect transistor (chemFET)<sup>26</sup> sensing modalities. However, the lower electrical charge conduction of porphyrins restricts the use of conductance-based sensing modalities.<sup>27</sup>

To overcome these issues, we have fabricated a microelectronic sensor device by aligning SWNTs on gold microelectrodes, and further functionalization of SWNTs with cobalt octaethyl porphyrin (CoOEP). Here, the one-dimensional (1D) nanostructure of SWNTs provides fast charge conduction and stable device performance with high sensitivity, while functionalization with CoOEP improves the selectivity of the sensor device to a specific group of analytes with high recovery since the analyte does not come into direct contact with SWNTs, which restricts trapping of analyte molecules inside the honeycomb structure of SWNTs.<sup>28</sup> CoOEP possesses cobalt as a central metal ion surrounded by organic ligands. The sensor device performance was evaluated by chemiresistive sensing modality and shows sensor response towards acetone, dichloromethane (DCM), methyl ethyl ketone (MEK), ethanol, and methanol at a low limit of detection (LOD) of 5 ppm with high sensitivity. Further, the data was analyzed with pattern recognition tools like principal component analysis (PCA) and linear discrimination analysis (LDA). The data exhibited the discriminating capability of the CoOEP-functionalized SWNT chemiresistive sensor towards these analytes. These exciting results show the fabricated sensor would be useful as an E-nose for these gas analytes without the need for an array of sensors.

## Experimental

---

### Materials and Chemicals

COOH-SWNTs having an average diameter of 1–2 nm, length of 3–8  $\mu\text{m}$ , and specific surface area of 350–450  $\text{m}^2/\text{g}$  were purchased from Nanoshel, USA. N,N-dimethylformamide (DMF) and cobalt octaethyl porphyrin (CoOEP) were procured from Sigma Aldrich. Acetone and

isopropyl alcohol were purchase from Molychem, India. AZ 5214e image reversal photoresist, AZ 400 K developer, and AZ 100 remover were purchased from Microchemicals, Germany. All the testing gas calibrated mixtures were purchased from Space Cryogases Pvt. Ltd., India.

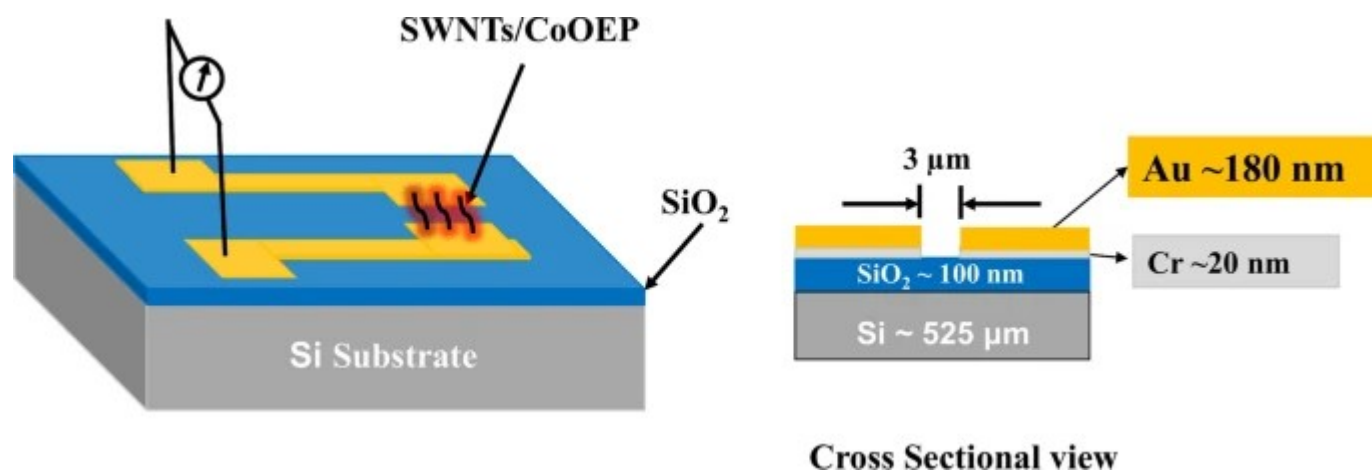
## Substrate Preparation and Device Fabrication

Gold electrodes (3- $\mu\text{m}$  gap) were prepared on silicon (Si)/silicon dioxide ( $\text{SiO}_2$ ) wafer by the photolithography method. Firstly, Si/ $\text{SiO}_2$  wafer was washed with acetone followed by isopropyl alcohol then dried using  $\text{N}_2$  flow and kept at  $120^\circ\text{C}$  for 2 min. AZ 5214e image reversal photoresist was spin-coated on Si/ $\text{SiO}_2$  wafer followed by pre-bake at  $100^\circ\text{C}$ . The photoresist-coated Si/ $\text{SiO}_2$  wafer was exposed to ultraviolet (UV) light through a mask aligner. Then the exposed wafer was developed in AZ 400 K developer solution and washed with deionized (DI) water and baked at  $120^\circ\text{C}$ . Chromium (20 nm) and gold (180 nm) were deposited on the developed Si/ $\text{SiO}_2$  wafer via E-beam and thermal coating method, respectively. The lift-off technique was used to develop the desired pattern using the AZ 100 remover solution.

The SWNT suspension was prepared in 10 ml of DMF by dispersing 0.2 mg of COOH-functionalized SWNTs by 90 min of ultrasonication (VWR, ultrasonicator) followed by centrifugation at 14,000 rpm to remove agglomerates, if any. The gap between two gold electrodes was bridged by aligning SWNTs dielectrophoretically as reported earlier.<sup>29</sup> The 0.1- $\mu\text{l}$  drop of SWNT suspension was drop-cast between two gold electrodes followed by applying 4-MHz frequency of  $1V_{\text{p-p}}$  signals using a function generator. After applying a drop of DI water, the electrodes were washed to remove unaligned SWNTs and dried using  $\text{N}_2$  gas flow gently. The prepared device was annealed in a reducing atmosphere (5%  $\text{H}_2$  + 95% Ar) at  $300^\circ\text{C}$  for 1 h to reduce the contact resistance and solvent molecules.

The solution of CoOEP was prepared in 0.1 mM DMF by ultrasonication for 30 min. The functionalization of aligned COOH-SWNTs was carried out by drop-casting a 0.1- $\mu\text{l}$  drop of CoOEP in DMF. The electrodes were dried at room temperature and used as a device; a schematic is shown in Fig. 1. The fabricated sensor device was soldered to a printed circuit board (PCB) using wedge wire bonder (WESTBOND, USA) and used for further electrical measurements.

Fig. 1



SWNTs/CoOEP sensor device prepared on a Si/SiO<sub>2</sub> wafer.

## Characterizations

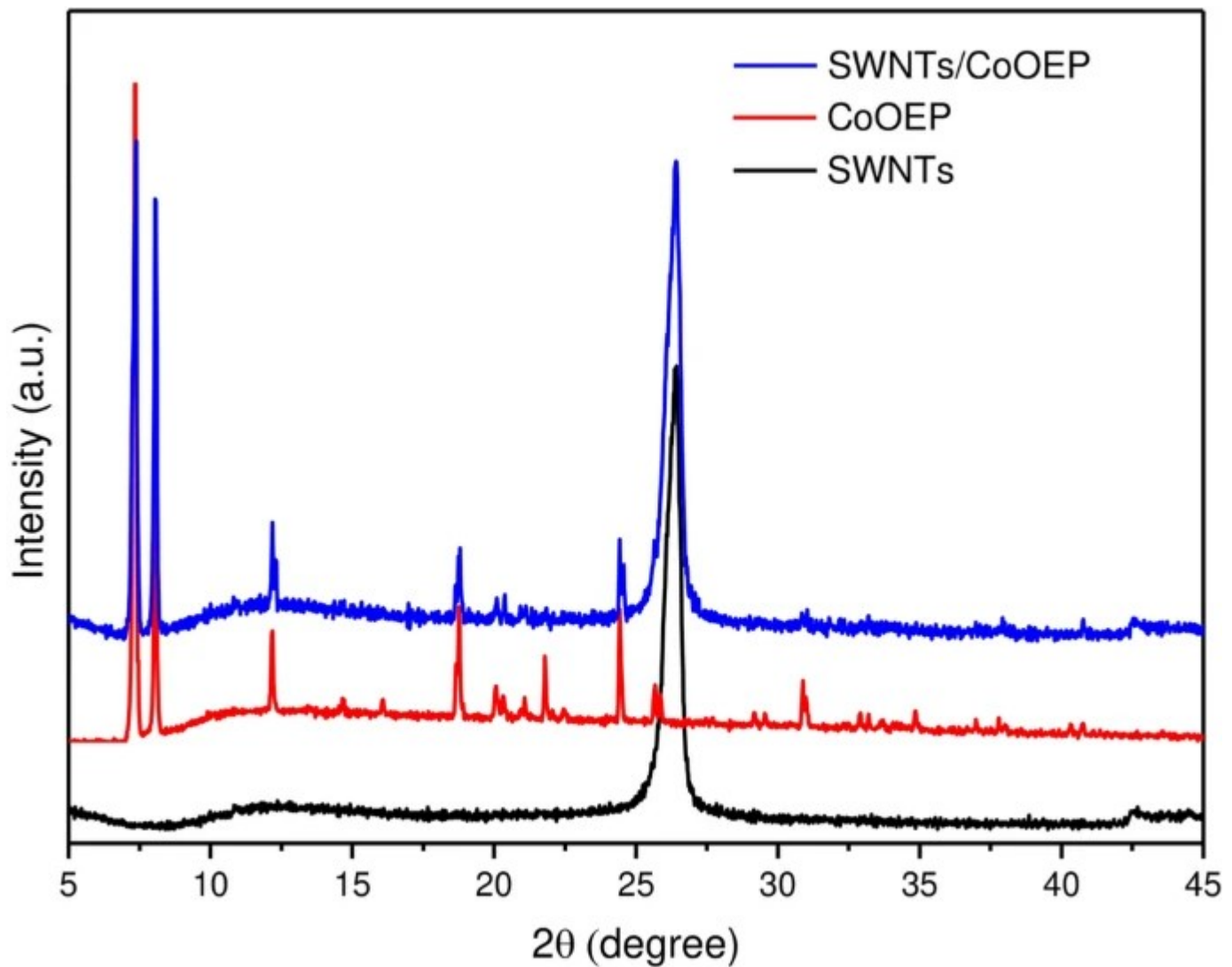
Fourier transform infrared (FTIR) spectroscopy of the CoOEP-functionalized COOH-SWNTs was carried out on a Bruker Alpha FTIR with an attenuated total reflection (ATR) attachment in the 500–4000-cm<sup>-1</sup> range. UV-visible spectroscopy of the samples was done using a Jasco V-750 spectrometer. Raman spectroscopy of the device was performed on an Xplora Plus Raman spectrometer (Horiba, France) at a 532-nm excitation wavelength with a ×50 objective. X-ray micro-diffraction measurements were performed on a Bruker D8 Advance instrument with a CuK $\alpha$  radiation source ( $\lambda = 1.544 \text{ \AA}$ ). Morphological characterization was carried out using a JEOL scanning electron microscope. Electrical characterizations ( $I$ - $V$ ) and chemiresistive sensing experiments were performed on a Keithley 4200A semiconductor analyzer at room temperature (27°C) in an in-house designed and developed dynamic gas sensing system. The gas chamber was specially designed from glass of 8-cc volume with inlet and outlet gas ports. Tedlar bags were filled with calibrated gases, maintaining a total flow rate of 200 sccm, and the concentration of gases was adjusted and controlled by computer-programmed Alicat mass flow controllers (MFCs) using dry air as carrier gas for the sensing experiment. The effect of relative humidity (RH) was measured on the same system only in place of the analyte, MFCs were connected to dry air and the output was introduced into a water bubbler, and saturated vapors were introduced. Humidity was measured by the calibrated humidity sensor and controlled by adjusting the flow rate of MFCs.

## Results and Discussion

### X-ray Diffraction

Figure 2 shows the x-ray diffraction (XRD) pattern of COOH-SWNTs, CoOEP, and aligned SWNTs functionalized with CoOEP (SWNTs/CoOEP). SWNTs<sup>30</sup> shows a (002) hkl plane at  $26^\circ$  and a (001) plane at around  $43^\circ$ , while SWNTs functionalized with CoOEP show both SWNT and CoOEP diffraction peaks, which confirms successful coating of the SWNTs with CoOEP.

Fig. 2

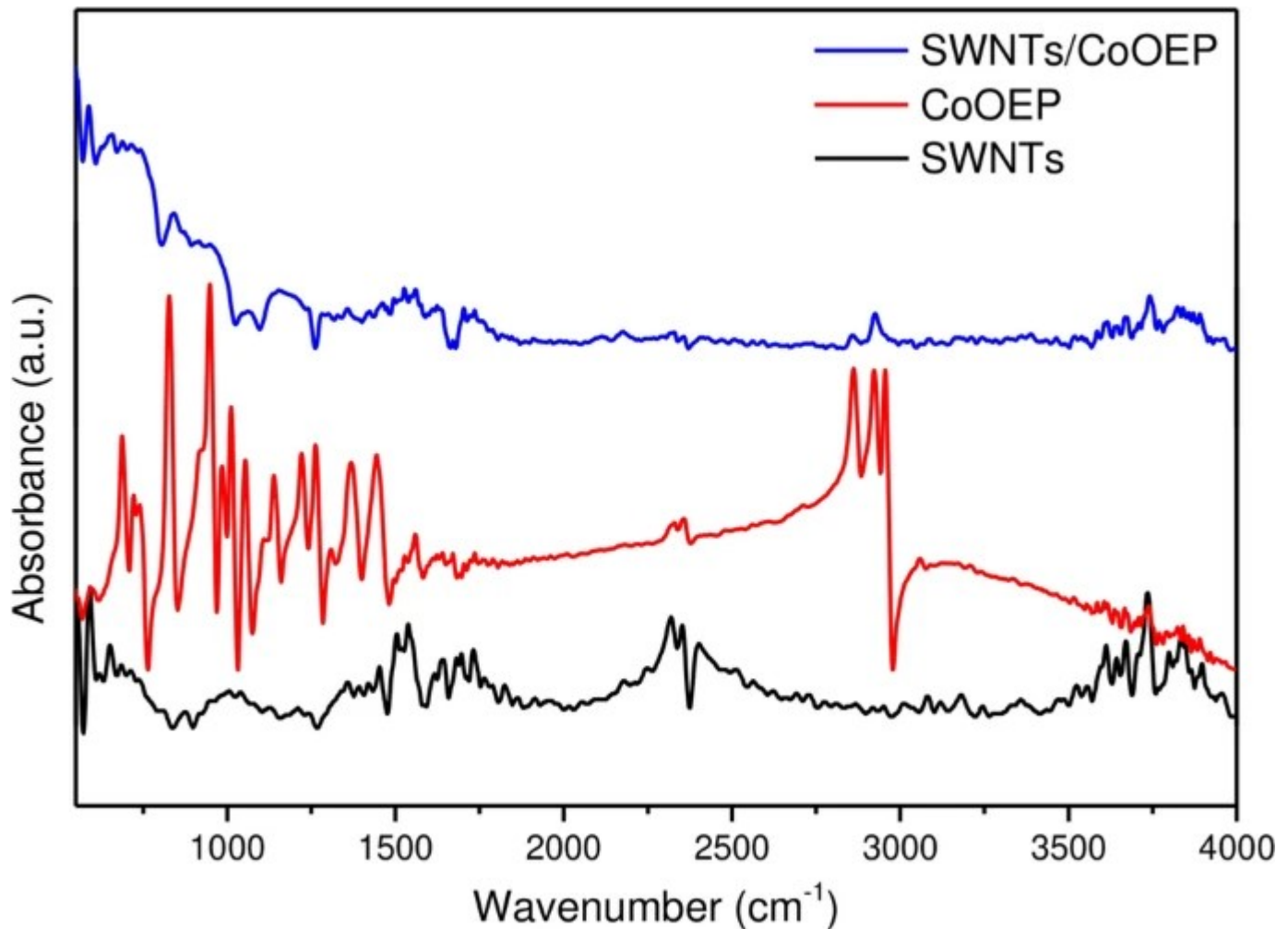


X-ray diffraction pattern of COOH-SWNTs, CoOEP, and SWNTs/CoOEP.

## Fourier Transform Infrared Spectroscopy

SWNTs, CoOEP, and SWNTs/CoOEP were characterized by FTIR spectroscopy as shown in Fig. 3. SWNTs show a peak at  $1730\text{ cm}^{-1}$  attributed to the C=O bond of attached -COOH functional group and a peak at  $1580\text{ cm}^{-1}$  assigned to C=C bond stretching mode of the nanotubes with a sidewall defect site.<sup>31</sup> CoOEP shows some characteristic peaks, one at  $742\text{ cm}^{-1}$  assigned to C-H out-of-plane bending in the benzene ring, and a peak at  $1135\text{ cm}^{-1}$  assigned to C-N stretching mode in porphyrin.<sup>32</sup> In SWNTs functionalized with CoOEP (SWNTs/CoOEP), porphyrin shows the presence of these characteristic peaks, which confirms successful functionalization of the SWNTs.

Fig. 3



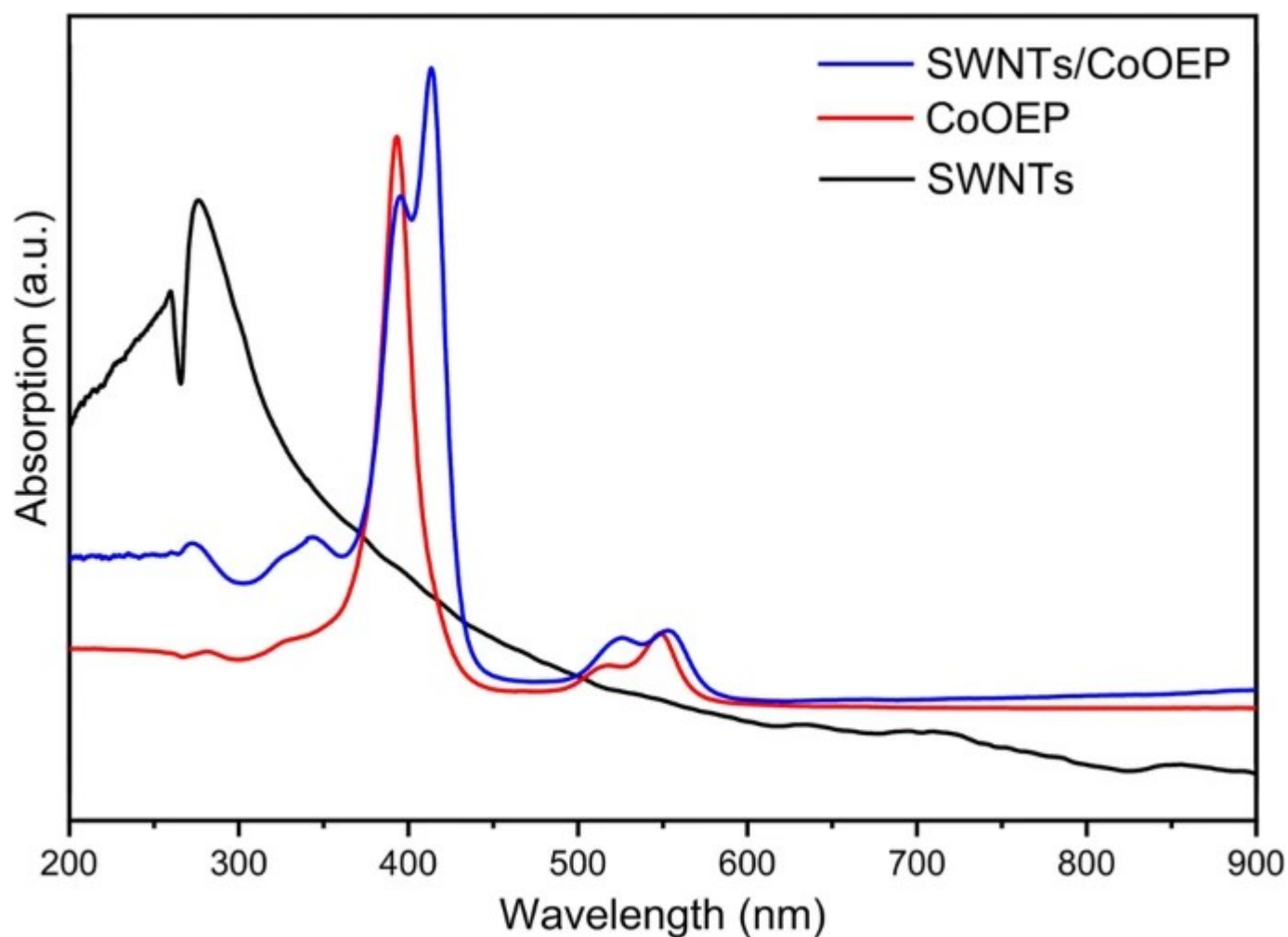
FTIR spectra of COOH-SWNTs, CoOEP, and SWNTs/CoOEP.



## UV–Visible Spectroscopy

UV–visible spectra of SWNTs, CoOEP, and SWNTs/CoOEP are shown in Fig. 4. SWNTs show absorption peaks at around 300 nm and 260 nm<sup>33</sup> which are assigned to plasmon absorption of SWNTs.<sup>34</sup> CoOEP shows electronic transition absorption at 390 nm, which can be assigned to the solet band; the peak at 550 nm with a shoulder at 520 nm corresponds to  $\alpha$ - and  $\beta$ -bands in Q-band vibrations.<sup>35</sup> SWNTs functionalized with CoOEP show extra electronic absorption peaks at 415 nm with a shoulder at 390 nm assigned to the solet band. The absorption peak observed for pristine CoOEP at 550 nm with a shoulder at 520 nm is also observed for CoOEP-functionalized SWNTs and is similarly assigned to the Q band of CoOEP, which confirms the successful functionalization of SWNTs with CoOEPs.

Fig. 4

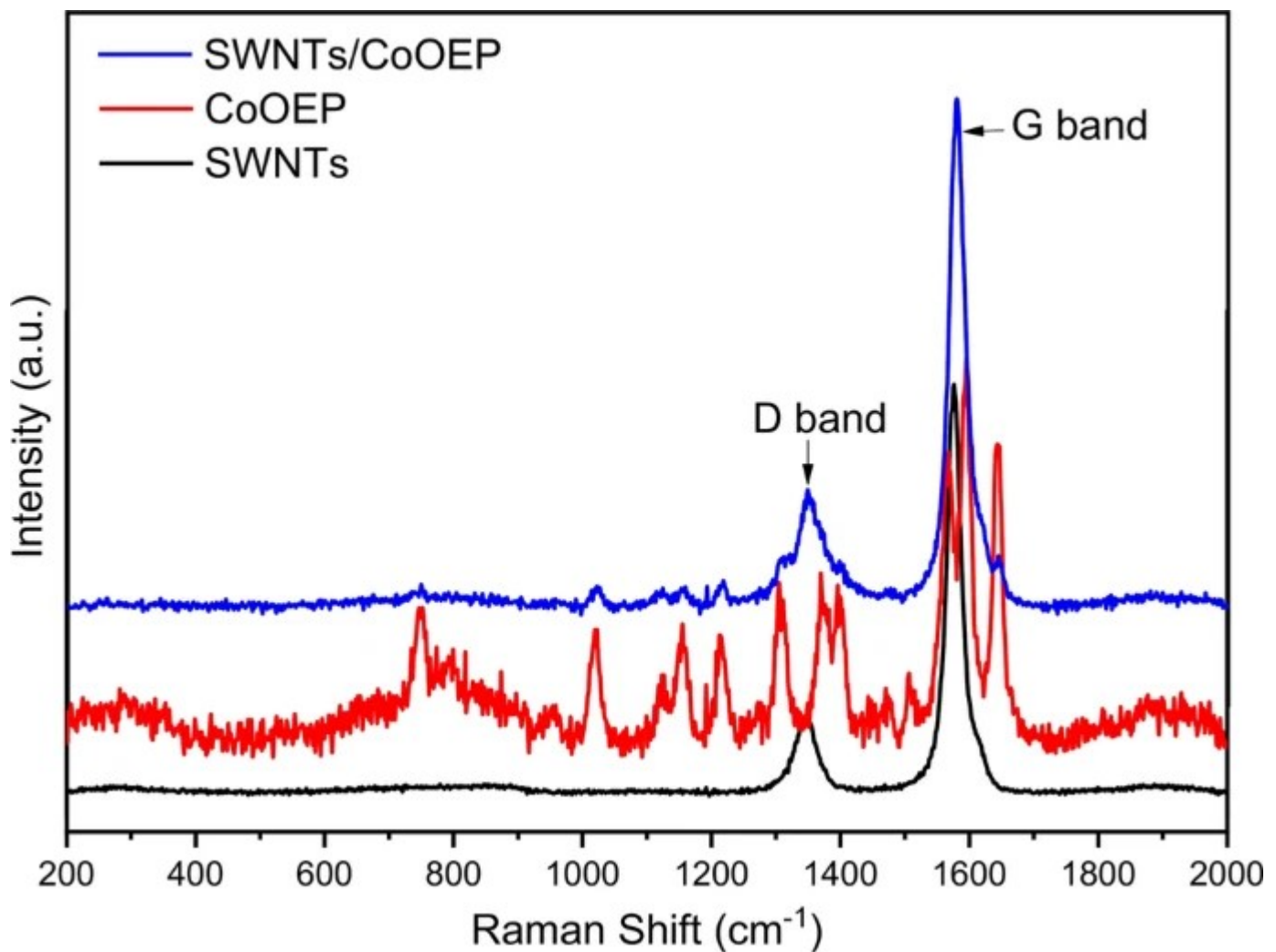


UV–visible spectra of COOH–SWNTs, CoOEP, and SWNTs/CoOEP.

## Raman Spectroscopy

Raman spectra of SWNTs, CoOEP, and CoOEP-functionalized SWNTs are shown in Fig. 5. The G-band and D-band, which are the main characteristic peaks for the confirmation of SWNTs, are seen in the Raman spectra of aligned pristine SWNTs<sup>36</sup> and CoOEP-functionalized SWNTs on the microelectrode device. The Raman spectra of pristine CoOEP and CoOEP-functionalized SWNTs show Raman shift at  $1000\text{ cm}^{-1}$ ,  $1580\text{ cm}^{-1}$ , and  $1600\text{ cm}^{-1}$ , assigned to  $\nu(\text{CC})$  aromatic ring chain vibrations, a peak shift at  $1610\text{--}1680\text{ cm}^{-1}$  corresponding to  $\nu(\text{C}=\text{N})$ , and a peak at  $1380\text{ cm}^{-1}$  corresponding to  $\delta(\text{CH}_3)$  vibrations present in the CoOEP chain.

Fig. 5

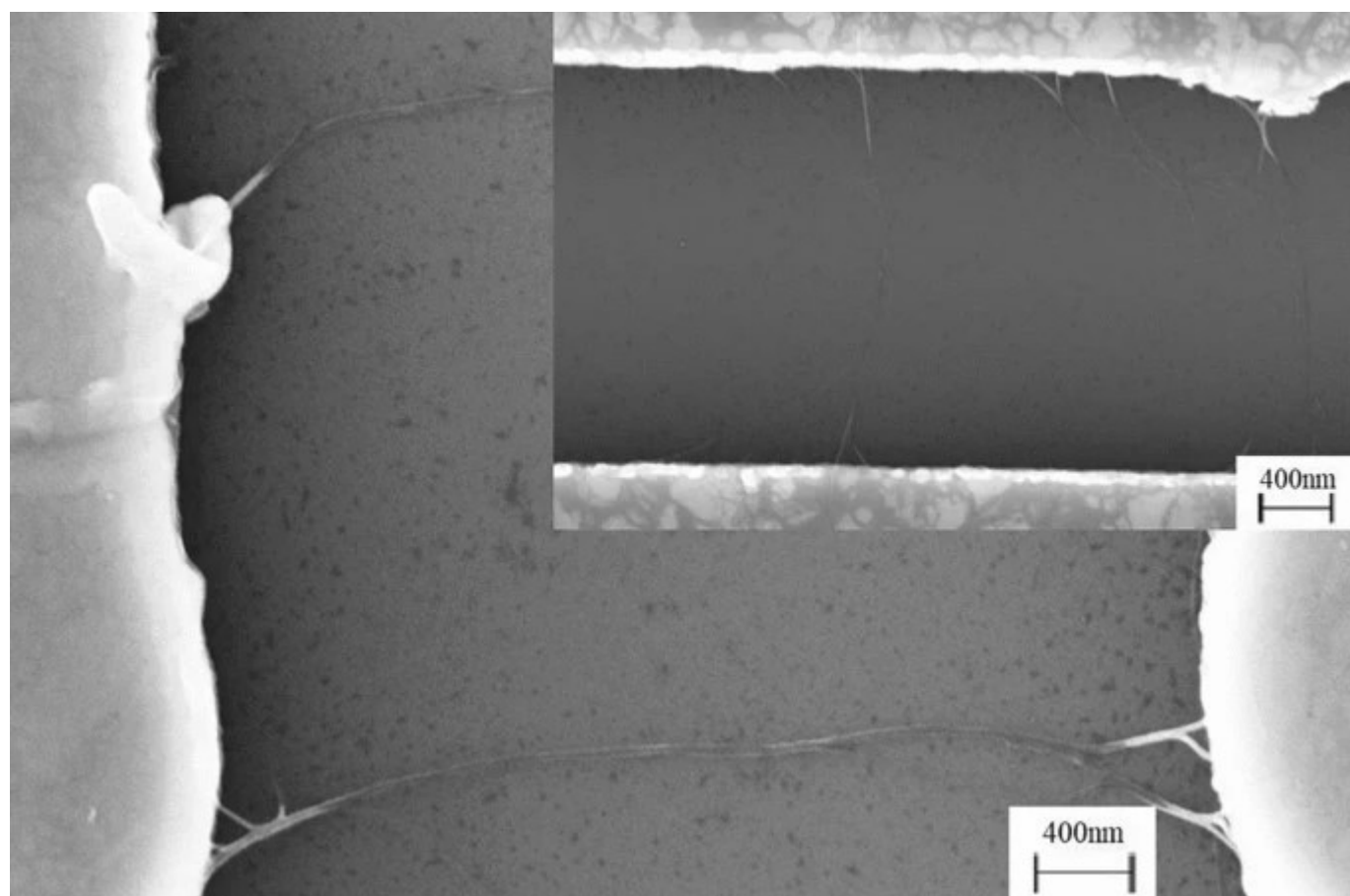


Raman spectra of COOH-SWNTs, CoOEP, and SWNTs/CoOEP.

## Scanning Electron Microscopy (SEM)

SEM images (Fig. 6) confirm the aligned bare SWNTs (inset) matrix between two gold electrodes successfully. Also, CoOEP-functionalized SWNTs show the uniform coating of SWNTs with CoOEP with an increase in diameter (c.a. 15–20 nm).

Fig. 6



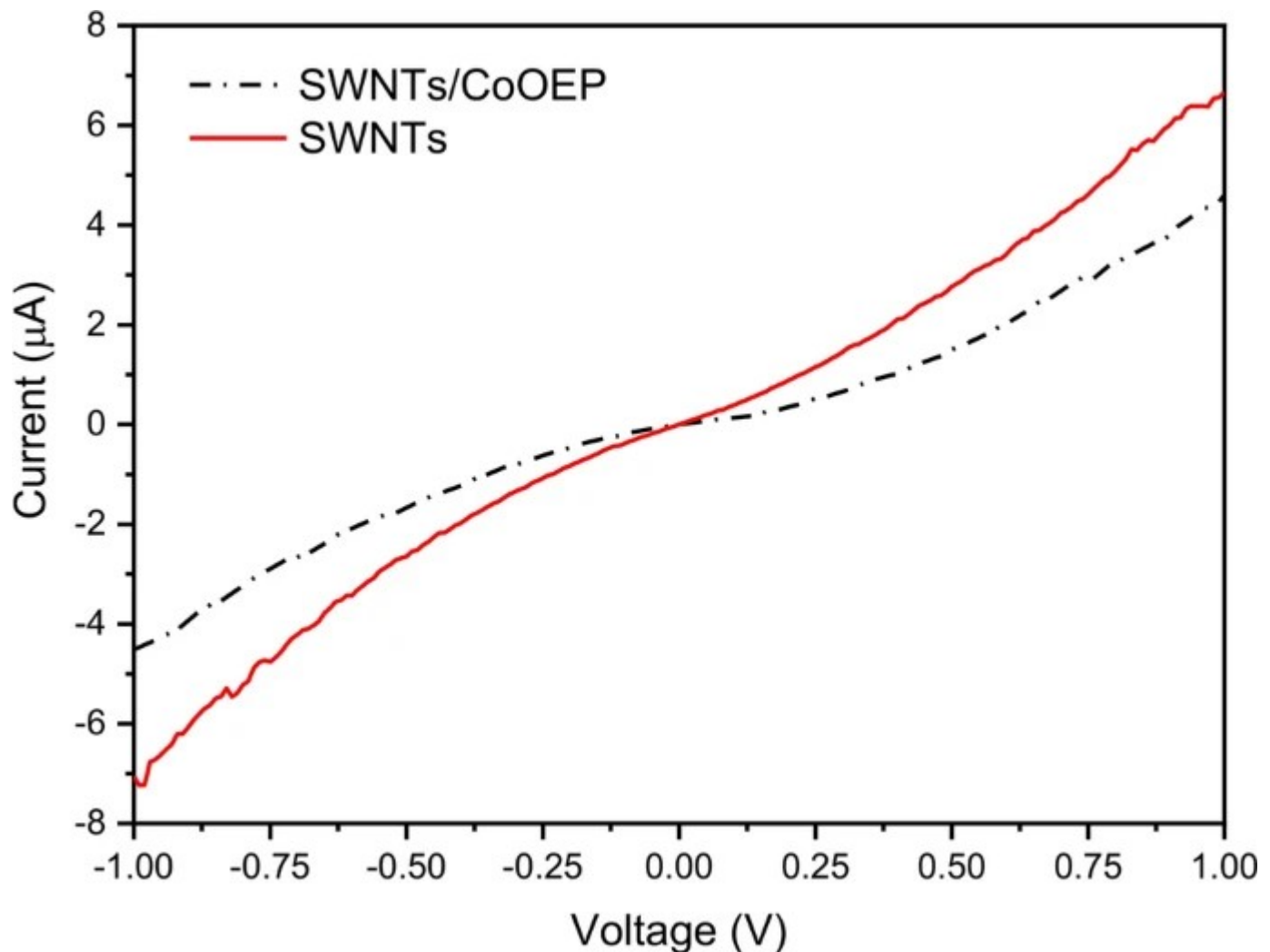
SEM images of CoOEP-functionalized SWNTs and aligned bare SWNTs (inset).

## $I$ – $V$ Characterization

Figure 7 shows electrical characterization ( $I$ – $V$  measurement) of bare SWNTs and SWNTs after functionalization with CoOEP (SWNTs/CoOEP). It shows (solid line) an increase in electrical resistance of aligned SWNTs after functionalization with CoOEP (SWNTs/CoOEP). This is due to the formation of a charge-transfer complex between SWNTs and CoOEP with  $\pi$ – $\pi$  interaction.<sup>37</sup> Used SWNTs show  $p$ -type nature when the device has formed since the  $I$ – $V$

graph shows S-shape curves and possesses a *p*-type nature.<sup>37</sup> CoOEP has an electron donor property, and when SWNTs are functionalized with CoOEP, it donates electrons to SWNTs, and the electron–hole combination leads to a decrease in charge carrier (hole) concentration in SWNTs.<sup>27,37,38</sup>

Fig. 7



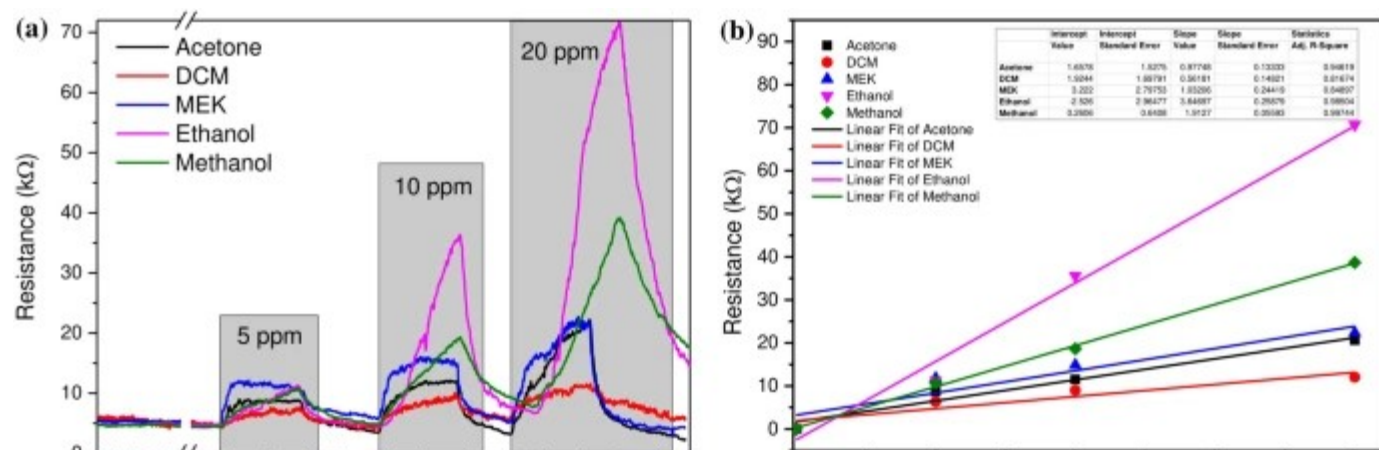
*I*–*V* characterization of bare COOH–SWNTs and SWNTs/CoOEP.

## Sensor Performance

The chemiresistive sensing performance of the SWNTs/CoOEP device is shown in Fig. 8a. The fabricated sensor shows response towards acetone, DCM, MEK, ethanol, and methanol vapors

up to 5 ppm of concentration below the permissible exposure limits (PELs) of these analytes, as shown in Table I. This shows the fabricated sensor device can be used as an E-nose. The device shows sensing response as a change in the resistance in the presence of gaseous analytes, and the change in resistance ( $R$ ) is shown in Fig. 8a. In the CoOEP-functionalized SWNT chemiresistor sensor, CoOEP interacts with HOOC-SWNTs, which forms a charge-transfer complex due to  $\pi$ - $\pi$  stacking. Metalloporphyrins are well-known electron donors, and SWNTs are a  $p$ -type material; therefore, after coating metalloporphyrins on SWNTs, metalloporphyrins will modulate the conductivity of SWNTs. When gaseous molecules come in contact with the SWNTs/CoOEP, the gas analyte molecules interact with the metalloporphyrin (i.e. CoOEP), and the electron-donating capability of metalloporphyrins is modulated, thereby modulating the conductivity of SWNTs underneath, which is directly proportional to the concentration of the gaseous analyte molecules. The fabricated sensor device has a very high reversible sensing response towards each concentration with a response and recovery time of 17 and 6 s, respectively. Further, Fig. 8b shows the calibration plot of the fabricated sensor device towards the VOC analytes and shows the highest sensitivity towards ethanol gas. The sensitivity of the device was calculated by the slope of the linear fit of the calibration plot with a very good fitting factor [adj.  $R$ -square ( $R^2$ )], as shown in Fig. 7b. The prepared chemiresistive sensor device shows reversible sensing performance with excellent recovery (up to >90%) for each analyte. The histogram (Fig. 9a) of the fabricated chemiresistive sensor device shows an excellent response towards each analyte (acetone, DCM, MEK, ethanol, and methanol) at various concentrations. Also, the device was tested with various humidity (RH) levels from 5% to 100% RH (Fig. 9b), and it shows negligible change in resistance as compared to the response towards gaseous analytes.

Fig. 8

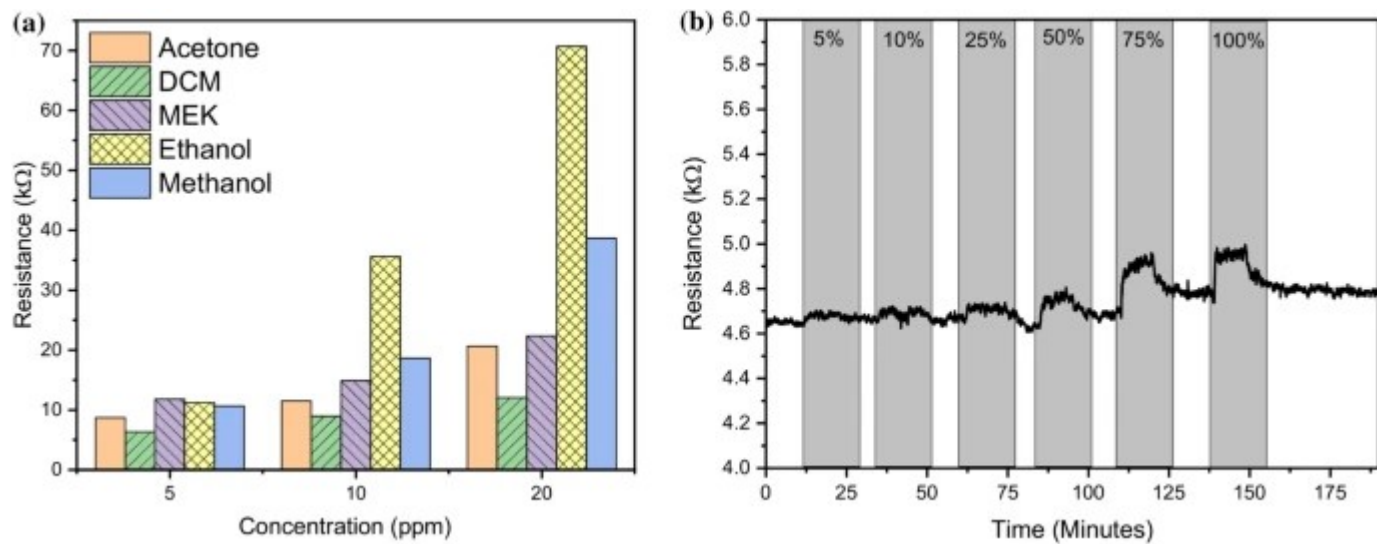




(a) CoOEP-functionalized SWNT chemiresistor sensor device response towards VOCs at a concentration of 5 ppm, 10 ppm, and 20 ppm. (b) Calibration plot of the sensor device towards VOCs (acetone, DCM, MEK, ethanol, and methanol).

Table I Chemiresistive sensor response towards each analyte (ppm) w.r.t. OSHA PEL (ppm)

Fig. 9



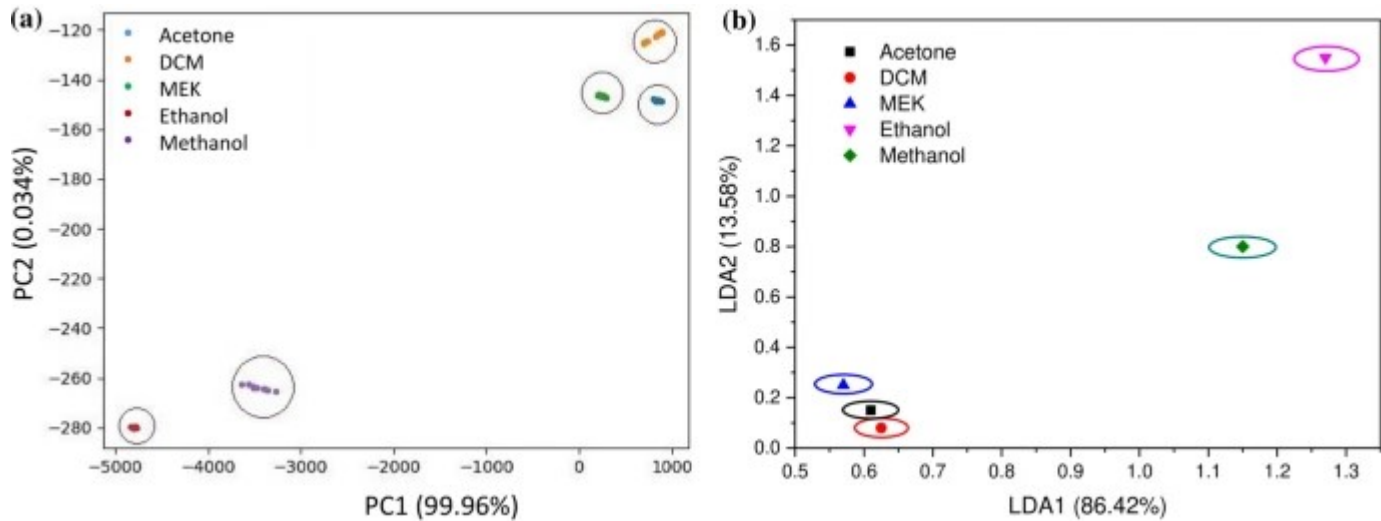
(a) Histogram of CoOEP-functionalized SWNT (SWNTs/CoOEP) chemiresistor sensor device response towards VOCs (acetone, DCM, MEK, ethanol, and methanol) at a concentration of 5 ppm, 10 ppm, and 20 ppm. (b) Response towards various humidity (RH) levels from 5% to 100% RH.

## Multivariate Analysis [Principal Component Analysis (PCA) and Linear Discriminant Analysis (LDA)]

Statistical tools were used to discern the response towards the different analyte gases.

Multivariate analysis was performed using principal component analysis (PCA) and linear discriminant analysis (LDA) as shown in Fig. 10a and b.

Fig. 10



(a) Principal component analysis (PCA) of the SWNTs/CoOEP sensor device. (b) Linear discrimination analysis (LDA) of the sensor device towards VOCs (acetone, DCM, MEK, ethanol, and methanol).

PCA focuses on analysis for linear dimension reduction and is used to obtain the key data characteristics. The decision of dimension reduction depends on the data itself. A set of vectors that can convey the original data are sought, and the occlusion of projections takes place from high-dimensional to low-dimensional space. This is unsupervised, whereas LDA is supervised. With the dimension reduction method, the data are projected in a low dimension. The projection points of each data type are hoped to be as near as possible and as wide as possible amongst the data type centers of various types. The group can be calculated by classifying a new sample based on the location of the previous sample projection point. The following is a summary of this particular algorithm.

## Principal Component Analysis

PCA can reduce the dimensions and convey the preliminary assessments of similarity between classes. PCA is a projection method that makes it easy to display all the information contained in a data set.

Figure 10a shows the classification of VOCs (acetone, DCM, MEK, ethanol, and methanol) by PCA in the case of steady-state response and mean value. In the steady-state case, the variance contribution rate of PCA1 was 99.97%, and PCA2 was 0.03%, and the total contribution rate of the first two PCs was 99%. In a two-dimensional graph, the distribution of sample points of DCM, acetone, ethanol, methanol, MEK can be seen. Therefore, the classification effect of PCA in the steady-state response is relatively poor. The five types of sample points have vast interclass distances in Fig. 9a.

## Linear Discriminant Analysis

Figure 10b presents the classification results of the VOCs (acetone, DCM, MEK, ethanol, and methanol) by LDA which are different in the case of steady-state response and mean value. The variance contribution rate of LDA1 is 86.42%, and LDA2 is 13.36%; the total contribution rate of the first two LDAs is 86.42%. Table II shows accuracy comparison of PCA and LDA. Thus, PCA classification is observed to be more efficient than LDA.

---

**Table II** The overall recognition accuracy of gases

---

These results show the fabricated SWNTs/CoOEP chemiresistive sensor could be used as an intelligent E-nose for selective and sensitive detection of acetone, DCM, MEK, ethanol, and methanol gases.

## Conclusions

---

In summary, a high-performance chemiresistive sensor device has been fabricated using single-walled carbon nanotubes (SWNTs) functionalized with cobalt octaethyl porphyrin (CoOEP) on the microelectrodes prepared on Si/SiO<sub>2</sub> substrate. The chemiresistor sensor shows excellent response towards various VOCs viz. acetone, DCM, MEK, ethanol, and methanol below the OSHA PEL limit with 17 s and 6 s of response and recovery time, respectively. Multivariate analysis carried out by PCA and LDA exhibits excellent discriminating capabilities of the SWNTs/CoOEP-based chemiresistor sensor for detection of



multiple analytes (viz. acetone, DCM, MEK, ethanol, and methanol), which could be used as an electronic nose (E-nose). The materials and the microsensor device were characterized rigorously using XRD, FTIR, UV–visible spectroscopy, Raman spectroscopy, and current–voltage ( $I$ – $V$ ) characteristics.

## References

---

1. M.D. Shirsat, M.A. Bangar, M.A. Deshusses, N.V. Myung, and A. Mulchandani, *Appl. Phys. Lett.* 94, 083502 (2009).

[Article](#) [Google Scholar](#)

2. J. Dai, O. Ogbeide, N. Macadam, Q. Sun, W. Yu, Y. Li, B.-L. Su, T. Hasan, X. Huang, and W. Huang, *Chem. Soc. Rev.* 49, 1756 (2020).

[Article](#) [CAS](#) [Google Scholar](#)

3. J.-H. Lee, A. Mirzaei, J.-Y. Kim, J.-H. Kim, H.W. Kim, and S.S. Kim, *Sens. Actuators B Chem.* 302, 127196 (2020).

[Article](#) [CAS](#) [Google Scholar](#)

4. V. Balasubramani, S. Chandraleka, T. Subba Rao, R. Sasikumar, M.R. Kuppusamy, and T.M. Sridhar, *J. Electrochem. Soc.* 167, 037572 (2020).

[Article](#) [CAS](#) [Google Scholar](#)

5. N.M. Santhosh, A. Vasudevan, A. Jurov, A. Korent, P. Slobodian, J. Zavašnik, and U. Cvelbar, *Microelectron. Eng.* 2020, 111403 (2020).

[Article](#) [Google Scholar](#)

6. M.G. Stanford, K. Yang, Y. Chyan, C. Kittrell, and J.M. Tour, *ACS Nano* 13, 3474 (2019).

[Article](#) [CAS](#) [Google Scholar](#)

7. M. Stefanelli, G. Magna, F. Zurlo, F.M. Caso, E. Di Bartolomeo, S. Antonaroli, M. Venanzi, R. Paolesse, C. Di Natale, and D. Monti, *ACS Appl. Mater. Interfaces* 11, 12077 (2019).

[Article](#) [CAS](#) [Google Scholar](#)

8. M.S. Dresselhaus, G. Dresselhaus, and Ph. Avouris. *Topics in applied physics* (Springer, Berlin, 2001).

9. S. Qiu, K. Wu, B. Gao, L. Li, H. Jin, and Q. Li, *Adv. Mater.* 31, 1800750 (2019).

[Article](#) [Google Scholar](#)

10. S. Park, Y. Byoun, H. Kang, Y.-J. Song, and S.-W. Choi, *ACS Omega* 4, 10677 (2019).

[Article](#) [CAS](#) [Google Scholar](#)

11. J.E. Ellis, Z. Zeng, S.I. Hwang, S. Li, T.-Y. Luo, S.C. Burkert, D.L. White, N.L. Rosi, J.J. Gassensmith, and A. Star, *Chem. Sci.* 10, 737 (2019).

[Article](#) [CAS](#) [Google Scholar](#)

12. F.A. Zubieta-López, J.A. Díaz-Celaya, S. Godavarthi, R. Falconi, E. Chigo-Anota, M. Salazar-Villanueva, F. Ortiz-Chi, and M. Acosta-Alejandro, *Diamond Relat. Mater.* 110, 108108 (2020).

[Article](#) [Google Scholar](#)

13. S. Kim, H.R. Lee, Y.J. Yun, S. Ji, K. Yoo, W.S. Yun, J.-Y. Koo, and D.H. Ha, *Appl. Phys. Lett.* 91, 093126 (2007).

[Article](#) [Google Scholar](#)

14. D.W.H. Fam, A.I.Y. Tok, A. Palaniappan, P. Noppawan, A. Lohani, and S.G. Mhaisalkar, *Sens. Actuators B Chem.* 138, 189 (2009).

[Article](#) [CAS](#) [Google Scholar](#)

15. Y. Seekaew, A. Wisitsoraat, D. Phokharatkul, and C. Wongchoosuk, *Sens. Actuators B Chem.* 279, 69 (2019).

[Article](#) [CAS](#) [Google Scholar](#)

16. P. Qi, O. Vermesh, M. Grecu, A. Javey, Q. Wang, H. Dai, S. Peng, and K.J. Cho, *Nano Lett.* 3, 347 (2003).

[Article](#) [CAS](#) [Google Scholar](#)

17. A.D. Rushi, K.P. Datta, P.S. Ghosh, A. Mulchandani, and M.D. Shirsat, *J. Phys. Chem. C* 118, 24034 (2014).

[Article](#) [CAS](#) [Google Scholar](#)

18. A. Rushi, K. Datta, P. Ghosh, A. Mulchandani, and M. Shirsat, *Physica status solidi (a)* 215, 1700956 (2018).

[Article](#) [Google Scholar](#)

19. M. Biesaga, K. Pyrzyńska, and M. Trojanowicz, *Talanta* 51, 209 (2000).

[Article](#) [CAS](#) [Google Scholar](#)

20. R.A. Ware, and J. Wei, *J. Catal.* 93, 100 (1985).

[Article](#) [CAS](#) [Google Scholar](#)

21. C. Di Natale, D. Monti, and R. Paolesse, *Mater. Today* 13, 46 (2010).

[Article](#) [Google Scholar](#)

22. P. Lorwongtragool, N. Boonyopakorn, and S. Kladsomboon, *J. Phys. Conf. Ser.* 2019, 012014 (2019).

[Article](#) [Google Scholar](#)

23. G Mamtmin, N Kari, R Abdurahman, P Nizamidin and A Yimit, *Optics & Laser Technology.* 128, 106260 (2020).

24. S. Ishihara, J. Labuta, W. Van Rossom, D. Ishikawa, K. Minami, J.P. Hill, and K. Ariga, *Phys. Chem. Chem. Phys.* 16, 9713 (2014).

[Article](#) [CAS](#) [Google Scholar](#)

25. Y. Wang, P. Ma, F. Song, S. Yao, C. Chen, and P. Zhu, *J. Colloid Interface Sci.* 490, 129 (2017).

[Article](#) [CAS](#) [Google Scholar](#)

26. C. Di Natale, K. Buchholt, E. Martinelli, R. Paolesse, G. Pomarico, A. D'Amico, I. Lundström, and A.L. Spetz, *Sens. Actuators B Chem.* 135, 560 (2009).

[Article](#) [Google Scholar](#)

27. M.D. Shirsat, T. Sarkar, J. Kakoullis Jr., N.V. Myung, B. Konnanath, A. Spanias, and A. Mulchandani, *J. Phys. Chem. C* 116, 3845 (2012).

[Article](#) [CAS](#) [Google Scholar](#)

28. T. Zhang, S. Mubeen, N.V. Myung, and M.A. Deshusses, *Nanotechnology* 19, 332001 (2008).

[Article](#) [Google Scholar](#)

29. K. Datta, P. Ghosh, M.A. More, M.D. Shirsat, and A. Mulchandani, *J. Phys. D Appl. Phys.* 45, 355305 (2012).

[Article](#) [Google Scholar](#)

30. P.K. Giri, and D.K. Singh, *J. Surf. Eng. Mater. Adv. Technol.* 3, 27316 (2013).

[Google Scholar](#)

31. B. Yue, Y. Wang, C.-Y. Huang, R. Pfeffer, and Z. Iqbal, *J. Nanosci. Nanotechnol.* 7, 994 (2007).

[Article](#) [CAS](#) [Google Scholar](#)

32. C.J. Verma, R.K. Pandey, and R. Prakash, *Mater. Sci. Eng. B* 227, 80 (2018).

[Article](#) [CAS](#) [Google Scholar](#)

33. Y. Shi, L. Ren, D. Li, H. Gao, and B. Yang, *J. Surf. Eng. Mater. Adv. Technol.* 3, 6 (2013).

34. X. Dong, Y. Tang, M. Wu, B. Vlahovic, and L. Yang, *J. Biol. Eng.* 7, 19 (2013).

[Article](#) [Google Scholar](#)

35. C. Zheng, L. Huang, W. Li, and W. Chen, *Appl. Phys. B* 123, 27 (2017).

[Article](#) [Google Scholar](#)

36. A.I. Lopez-Lorente, B.M. Simonet, and M. Valcárcel, *Analyst* 139, 290 (2014).

[Article](#) [CAS](#) [Google Scholar](#)

37. D.R. Kauffman, O. Kuzmych, and A. Star, *J. Phys. Chem. C* 111, 3539 (2007).

[Article](#) [CAS](#) [Google Scholar](#)

38. M.E. Itkis, S. Niyogi, M.E. Meng, M.A. Hamon, H. Hu, and R.C. Haddon, *Nano Lett.* 2, 155 (2002).

[Article](#) [CAS](#) [Google Scholar](#)

## Acknowledgments

---

The authors extend their sincere thanks to UGC-DAE CSR (RRCAT), Indore (Project No. CSR-IC-BL66/CRS-183/2016-17/847), Inter University Accelerator Center (IUAC), New Delhi, India (UFR No. 62320), DST-SERB, New Delhi (Project No. EEQ/2017/000645), Rashtriya Uchachatar Shiksha Abhiyan (RUSA), Government of Maharashtra, UGC-SAP Programme (F.530/16/DRS-I/2016 (SAP-II) Dt. 16-04-2016), and DST-FIST (Project No. SR/FST/PSI-210/2016(C) dtd. 16/12/2016) for providing financial support.

## Author information

---

Sumedh M. Shirsat and Gajanan A. Bodkhe have contributed equally to this work.

## Authors and Affiliations

Department of Electronics & Telecommunication Engineering, Jawaharlal Nehru Engineering College, Aurangabad, MS, 431 001, India

Sumedh M. Shirsat

RUSA Center for Advanced Sensor Technology, Department of Physics, Dr. Babasaheb Ambedkar Marathwada University, Aurangabad, MS, 431 004, India

Gajanan A. Bodkhe & Mahendra D. Shirsat

Department of Computer Science & Information Technology, Dr. Babasaheb Ambedkar Marathwada University, Aurangabad, MS, 431 004, India

Minakshi M. Sonawane & Bharti W. Gawali

## Corresponding author

Correspondence to [Mahendra D. Shirsat](#).

## Ethics declarations

---

## Conflict of interest

On behalf of all authors, the corresponding author states that there is no conflict of interest.

## Additional information

---

## Publisher's Note

Springer Nature remains neutral with regard to jurisdictional claims in published maps and institutional affiliations.

# Rights and permissions

---

[Reprints and permissions](#)

## About this article

---

### Cite this article

Shirsat, S.M., Bodkhe, G.A., Sonawane, M.M. *et al.* Multivariate Analysis of a Cobalt Octaethyl Porphyrin-Functionalized SWNT Microsensor Device for Selective and Simultaneous Detection of Multiple Analytes. *J. Electron. Mater.* 50, 5780–5787 (2021). <https://doi.org/10.1007/s11664-021-09111-3>

Received  
23 March 2021

Accepted  
02 July 2021

Published  
22 July 2021

Issue Date  
October 2021

DOI  
<https://doi.org/10.1007/s11664-021-09111-3>

### Share this article

Anyone you share the following link with will be able to read this content:

[Get shareable link](#)

Provided by the Springer Nature SharedIt content-sharing initiative

### Keywords

[Single-walled carbon nanotubes \(SWNTs\)](#)

[cobalt octaethyl porphyrin \(CoOEP\)](#)

[functionalization](#)

[principal component analysis \(PCA\)](#)



[linear discrimination analysis \(LDA\)](#)

[electronic nose \(E-nose\)](#)